NMR study of the 3*d* ferromagnetic metals: Critical region and paramagnetic phase

M. Shaham,* J. Barak, and U. El-Hanany
Soreq Nuclear Research Center, Yavne, Israel

W. W. Warren, Jr.
Bell Laboratories, Murray Hill, New Jersey 07974

(Received 27 May 1980)

The ferromagnetic transition metals iron, nickel, and cobalt have been investigated by nuclear magnetic resonance up to the critical region and, in the case of nickel and cobalt, in the paramagnetic phase. The measurements include the zero-field resonant frequency, spin-spin relaxation rate, and spin-lattice relaxation rate in the ferromagnetic phase, and the Knight shift and spin-lattice relaxation rate in the paramagnetic phase. The data yield values of the static critical exponent (β) for the spontaneous magnetization and the dynamic exponent (z) for spin fluctuations near the critical points of all three ferromagnetic metals. Paramagnetic-phase data for nickel and cobalt yield the d-spin hyperfine coupling and the orbital Knight shift and susceptibility contributions. Magnetic equation-of-state parameters are derived for nickel and cobalt. Noncritical spin-spin relaxation rates in the ferromagnetic phase are attributed mainly to Suhl-Nakamura interactions, but in bulk metal samples the rates exhibit a striking and unexplained maximum between room temperature and the critical point.

I. INTRODUCTION

The ferromagnetic transition metals iron, nickel, and cobalt are among the most familiar and useful of magnetic materials. Yet a satisfactory understanding of the origin and nature of ferromagnetism in these metals continues to be elusive. Their electronic and magnetic properties are characterized by the coexistence of features suggesting both localized and itinerant electronic states,[1,2] and much current theoretical effort is focused on reconciliation of these apparently contradictory concepts.[3] In this regard, phenomena associated with the magnetic phase transition and the electronic structure of the paramagnetic phase, together with the ferromagnetic ground state, represent particularly important subjects for study.

From the time of the discovery of the ^{59}Co nuclear magnetic resonance (NMR) in cobalt metal,[4] NMR has proven to be a valuable probe of the microscopic electronic and magnetic properties of the ferromagnetic transition metals. All three metals have been extensively studied in the ferromagnetic state near and below room temperature, i.e., well below the critical temperature T_c. It is natural to consider extension of such studies to the region of the critical point and to the paramagnetic state. NMR studies of critical spin fluctuations near T_c are of interest both within the general context of spin-fluctuation phenomena in three-dimensional isotropic ferromagnets and because these particular systems provide the opportunity to observe critical dynamics in strong itinerant ferromagnets. NMR data in the paramagnetic state can reveal details of the electronic structure which may be compared with the ferromagnetic state and with other nonmagnetic transition metals.

In spite of these motivations, previous NMR studies of the ferromagnetic transition metals at elevated temperatures have not reached the vicinity of T_c.[5–9] The reason for this is broadening of the NMR line which increases with temperature and eventually renders the resonance unobservable. When standard experimental methods are employed, this occurs far below T_c. However, recent work[10,11] has shown that the source of the most serious broadening is the temperature inhomogeneity across the sample. With sufficient care taken to reduce temperature inhomogeneities and by applying spin-echo techniques to work in the presence of residual inhomogeneities, it has been found possible to observe the NMR in iron, nickel, and cobalt up to within a few degrees of T_c—well into the critical regions.[11–13] Similar techniques permit observation of the NMR signals in paramagnetic nickel and cobalt.[10,11,13–15]

In this paper we report the results of a comprehensive high-temperature NMR investigation of iron, cobalt, and nickel. The data include the resonant field in the ferromagnetic state in zero applied field, the Knight shift in the paramagnetic state, and the nuclear spin-lattice and spin-spin relaxation times.

The temperature range extends from room temperature up to the critical region for all three metals and to the paramagnetic state of nickel and cobalt. We were unable to observe the ^{57}Fe NMR in paramagnetic iron. Because of the use of large applied fields above T_c and the inability to observe the NMR signals on approaching close to T_c from above, measurements in paramagnetic nickel and cobalt were limited to noncritical phenomena. Preliminary reports of these experiments have appeared elsewhere.[10–13]

The remainder of this paper is organized as follows. In Sec. II, we present details of the experimental apparatus and techniques. Sections III and IV contain experimental results and discussion of the resonant frequency in the ferromagnetic state, and the Knight shift in the paramagnetic state, respectively. In Sec. V these results are combined and fitted to a magnetic equation of state for nickel and cobalt. Section VI contains the observed nuclear relaxation rates, both the background rates far from T_c and the critical relaxation near T_c in the ferromagnetic states. Finally, we summarize in Sec. VII the principal results of the investigation.

II. EXPERIMENTAL APPARATUS AND TECHNIQUES

The main obstacle to observing NMR close to T_c is the strong temperature dependence of the NMR frequency in the critical region. As we discuss in detail in the following section, the NMR frequency in the ferromagnetic phase varies with temperature according to $(T_c - T)^{\beta}$. A temperature inhomogeneity, characterized by a gradient ΔT over the sample thus causes an inhomogeneous linewidth proportional to $\Delta T(T_c - T)^{\beta-1}$. Since $\beta < 1$, the linewidth diverges at T_c. The situation is similar in the paramagnetic state where the NMR frequency varies with temperature like the susceptibility (see Sec. IV). Thus the inhomogeneous linewidth in the paramagnetic state diverges according to $\Delta T(T - T_c)^{-(\gamma+1)}$ where γ is the critical exponent for the susceptibility ($\gamma > 1$).

In order to minimize this problem, furnaces were built which had very low temperature gradients (< 0.1 K/cm) across the sample region.[16,17] Thermal homogeneity was further improved by the use in most experiments of bulk polycrystalline samples whose intrinsic thermal conductivity was much higher than conventional dispersed powder samples. The furnaces were calibrated for the best temperature homogeneity conditions in the presence of the high rf power needed for NMR in the paramagnetic state and with the low rf power used in the ferromagnetic state where the rf magnetic field is enhanced.

Sample temperatures were measured with Pt vs Pt-Rh thermocouples placed adjacent to the sample containers. The temperature measurements were calibrated for the two rf power conditions by the change in the Q of the NMR coil at T_c for nickel and cobalt and also, in the case of cobalt, by the jump in the Knight shift at the melting point (Sec. IV). The thermocouple correction for nickel at T_c was 2.6 K under low rf power conditions and increased to 4.5 K at the high rf power level due to heating of the sample by the applied rf power. As an additional check on rf heating effects, we determined that the change of apparent Knight shift in paramagnetic cobalt corresponded to less than a 1 K change when the rf power was increased by a factor of 3 at 1300 K. For measurements on ferromagnetic iron, the thermocouple was not calibrated independently. The intrinsic calibration achieved by a power law fit to the resonant frequency (Sec. III) yielded a value of T_c 8° lower than the accepted value.

For measurements in the paramagnetic phase of cobalt a bulk polycrystalline sample was prepared by melting cobalt power (Spex 99.9999%). It was contained in an alumina ampoule around which the NMR coil was wound. Preliminary measurements[10] using a powdered sample yielded somewhat poorer signal-to-noise ratios due to the thermal inhomogeneity effect described above. A fixed frequency of 18.7 MHz was used with applied fields in the range 19–22 kOe. For measurements in the ferromagnetic phase, cobalt powder (Leico Industries Inc. 99.9999%) was mixed with alumina powder and sealed under argon in a quartz ampoule. The powder had a better signal-to-noise ratio than the bulk material in this case due to the relatively high resonant frequencies and small skin depth in ferromagnetic cobalt. We could observe the NMR of ^{59}Co in fcc cobalt in the absence of an applied magnetic field from 213 MHz at room temperature down to 52 MHz at 1385 K where we lost the signal because of the very short $T_2(< 1\ \mu\text{sec})$.

Measurements in both the ferromagnetic and paramagnetic phases of nickel were carried out on a bulk toroidal piece prepared from isotopically enriched ^{61}Ni (92.9%). This sample was sealed into a toroidal quartz ampoule with the rf coil wrapped around it so that the magnetic force lines were almost uniform around the toroidal inner and outer faces and perpendicular to its axis. The field H_0 of the superconducting magnet was parallel to this axis as needed for NMR experiments. A high filling factor was achieved in this way since the effective volume for the rf field included only the quartz walls and the sample skin depth (~ 0.1 mm at 20 MHz) and excluded the sample bore. The bore afforded a good place for the thermocouple element. The toroidal shape keeps the rf field lines closed in the coil and gives axial symmetry which is important for temperature homogeneity. Additional measurements were made below the critical region of ferromagnetic nickel using a bulk toroidal sample of natural isotopic abun-

dance and with powdered samples of both natural and enriched isotopic abundance. NMR signals in the range 4–26 MHz were observed with no applied magnetic field in the ferromagnetic phase. In paramagnetic nickel, a fixed frequency of 17 MHz was employed with applied fields in the range 44–50 kOe. The applied magnetic fields were calibrated by observing the ^{27}Al NMR signal in alumina.

Measurements in ferromagnetic iron were carried out using both powdered and bulk polycrystalline samples prepared from material enriched to 93.6% ^{57}Fe. Because of the higher melting point of iron, a toroidal sample was not prepared as was done for nickel. Rather, a conventional cylindrical configuration was employed. Both powdered and bulk iron samples were sealed under vacuum in quartz ampoules. Near T_c only the bulk sample yielded observable NMR signals. The zero-field ^{57}Fe resonance was observed from 45.6 down to 10.8 MHz.

III. NUCLEAR FERROMAGNETIC RESONANT FREQUENCY

The NMR frequency in the ferromagnetic phase was measured in iron in the range $288 \leq T \leq 1030$ K($\epsilon_- \equiv 1 - T/T_c \geq 4 \times 10^{-3}$), in fcc cobalt in the range $298 \leq T \leq 1385$ K($\epsilon_- \geq 7 \times 10^{-3}$) and in nickel in the range $423 \leq T \leq 631$ K($\epsilon_- \geq 2 \times 10^{-3}$). These frequencies, as measured for samples under their own vapor pressures, are plotted against temperature in Figs. 1(a), 1(b), and 1(c), respectively.

The contributions to the internal hyperfine field are proportional to the mean magnetic moment per atom[18] and thus to the magnetization M. Hence in the ferromagnetic phase, in the absence of an external magnetic field, the resonant frequency is given by

$$\nu = CM \quad . \tag{1}$$

Close to T_c, where variations of the proportionality constant C are negligible, $\nu(T)/\nu_0 = M(T)/M_0 = B\epsilon_-^{\beta}$ where ν_0 and M_0 are the resonant frequency and the magnetization at 0 K. A least squares fit of $\nu(T)$ to the power law with T_c as a parameter yielded the values of the parameter B, the critical exponent β and T_c given in Table I.

Our results for nickel are compared in Table I with other values obtained with pure nickel, i.e., with those measurements which do not utilize impurity atoms as probes of the local hyperfine field. These are the results of Cohen and Carver[19] from microwave transmission, the steady-state NMR results of Rotter and Sedlak,[9] and the results of Bleck *et al.*[20] who employed the method of perturbed angular distributions of γ rays using ^{63}Ni in the nickel host. With the exception of the steady-state NMR studies[9] which did not approach closer to T_c than

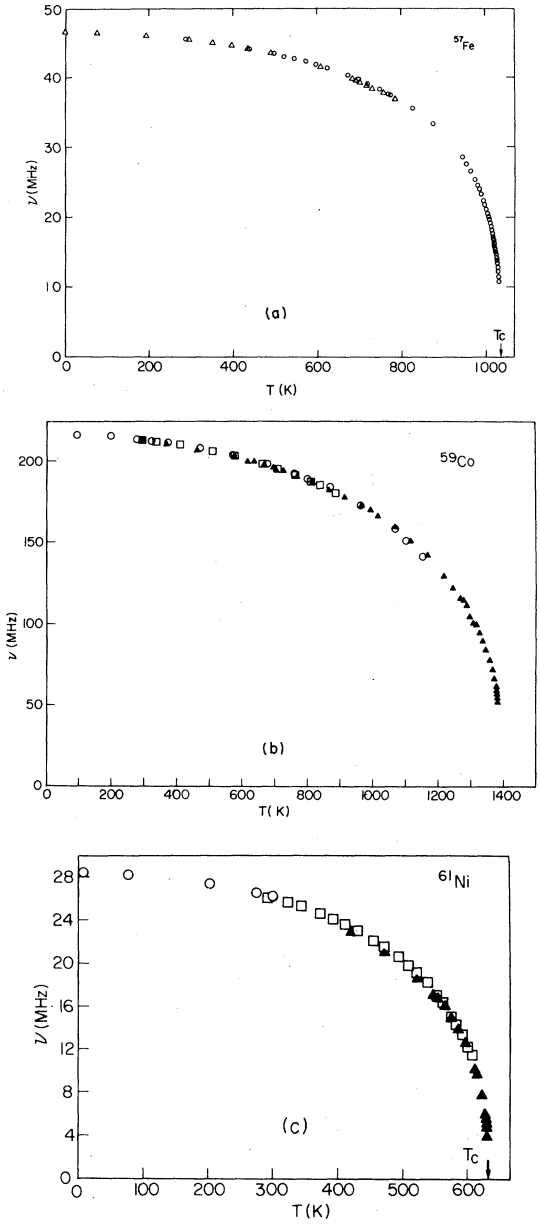

FIG. 1. NMR frequencies vs temperature in the ferromagnetic state of the 3d metals. (a) ^{57}Fe in bcc iron metal: O—present data; Δ—Budnick *et al.* (Ref. 5). (b) ^{59}Co in fcc cobalt metal: Δ—present data; O—Kôi *et al.* (Ref. 6); □—Conley *et al.* (Ref. 7). (c) ^{61}Ni in nickel metal: Δ—present data; □—Rotter and Sedlak (Ref. 9) CW measurements in natural Ni; O—Streever and Bennett (Ref. 8).

$\epsilon_- = 4 \times 10^{-2}$, the experiments on pure nickel yield values of β which are in agreement within experimental error. These results lie in the range $\beta = 0.34 \pm 0.02$ and are clearly lower than those obtained by the most accurate impurity hyperfine studies. The latter yield values close to $\beta = 0.38$.[21,22] It is

TABLE I. Power-law parameters for the critical behavior of the spontaneous magnetization at constant pressure.

Metal	Reference	B	β	T_c (K)	Range
Iron	Present work	1.35±0.02	0.320±0.004	1034.2 ±0.2	$4\times10^{-3}\leq\epsilon_-\leq5\times10^{-2}$
	Kobeissi and Hohenemser[a]	1.66±0.03	0.379±0.004	1042.91±0.04	$10^{-3}\leq\epsilon_-\leq2\times10^{-2}$
	NBS[b]	...	...	1042 ±4	
Cobalt	Present work	1.11±0.05	0.309±0.012	1394.9 ±1.0	$7\times10^{-3}\leq\epsilon_-\leq5\times10^{-2}$
	NBS[b]	...	...	1394 ±3	
Nickel	Present work	1.25±0.05	0.354±0.014	632.7 ±0.4	$2\times10^{-3}\leq\epsilon_-\leq10^{-1}$
	Cohen and Carver[c]	1.23±0.03	0.358±0.003	632.7 ±0.1	$5\times10^{-3}\leq\epsilon_-\leq10^{-1}$
	Bleck *et al.*[d]		0.322±0.016		
	Rotter and Sedlak[e]	...	0.338±0.002	630.8	$4\times10^{-2}\leq\epsilon_-\leq10^{-1}$
	NBS[b]	...	...	631 ±3	

[a]Reference 24.
[b]G. C. Carter, L. H. Bennett, and D. J. Kahan, *Metallic Shifts in NMR* (Pergamon, Oxford, 1977).
[c]Reference 19.
[d]Reference 20.
[e]Reference 9.

tempting to ascribe this difference to the effect of the impurity atom on the local hyperfine field. Bleck *et al.* found, in fact, that the apparent value of β was substantially higher in ^{66}Cu*Ni* and ^{67}Zn*Ni* than in ^{63}Ni*Ni*.[20] However, it must be noted that impurity hyperfine-field studies in nickel have been extended much closer to T_c than the pure nickel experiments and, further, that inclusion of data closer to T_c tends to change the value of β. This "range of fit" effect has been considered in detail by Suter and Hohenemser.[23] At the present time we believe that the relative importance for the value of β of impurity atoms and range of fit remains an open question. This point could be settled by accurate measurements on pure nickel closer to T_c than has been possible so far.

Although there have been fewer determinations of β for iron, we note that a discrepancy similar to that for nickel exists between our results and those of Mössbauer measurements of ^{57}Fe in iron.[24] The range of the Mössbauer experiments extends somewhat closer to T_c than our work but a sample with radioactive ^{57}Co impurities was used as source of γ rays.

Our result for cobalt is to the best of our knowledge the only zero-field measurement so far. Magnetization measurements at high magnetic field yielded $\beta=0.42\pm0.01$,[25] well above our value.

Equation (1) holds as long as there is no change in the hyperfine coupling due, say, to changes of the sample volume. However, the temperature dependences of the frequency and magnetization $\nu(T)$ and $M(T)$ were measured at constant pressure while the volume changed due to thermal expansion. This suggests[8] why plots of $\nu(T)/\nu_0$ and $M(T)/M_0$ vs T/T_c differ by more than 6% for nickel as shown in Fig. 2(a). Using the thermodynamic equation[26]

$$\left(\frac{\partial\ln\nu}{\partial T}\right)_V=\left(\frac{\partial\ln\nu}{\partial T}\right)_P-\left(\frac{\partial\ln\nu}{\partial P}\right)_T\left(V\frac{\partial P}{\partial V}\right)_T\frac{1}{V}\left(\frac{\partial V}{\partial T}\right)_P \quad (2)$$

$\nu(T)$ and $M(T)$ were corrected to constant volume values resulting in a residual deviation of $\sim3\%$ between the $\nu(T)/\nu_0$ and $M(T)/M_0$ curves for nickel shown in Fig. 2(b). The parameters used are given in Table II.

In cobalt $(\partial\ln M/\partial P)_T=-2.18\times10^{-4}$ (kbar)$^{-1}$ was measured[27] in the hexagonal phase. We assume that it is equal in the cubic phase due to the similar magnetic behavior of the two phases, and the comparable values for the other two cubic ferromagnets $(\partial\ln M/\partial P)_T^{\mathrm{Fe}}=-3.1\times10^{-4}$ (kbar)$^{-1}$ and $(\partial\ln M/\partial P)_T^{\mathrm{Ni}}=-2.9\times10^{-4}$ (kbar)$^{-1}$.[28] Moreover, it was found that Eq. (2) is not very sensitive to changes in the pressure dependence of M. Thermal expansion data were taken from Nix and MacNair[29] for nickel and from Müller and Scholten[30] for cobalt.

The near coincidence of $\nu(T)/\nu_0$ and $M(T)/M_0$ shows that the hyperfine coupling, C of Eq. (1), has only a very weak explicit temperature dependence for nickel and cobalt. Thus $\nu(T)$ at constant volume essentially represents the behavior of the magnetiza-

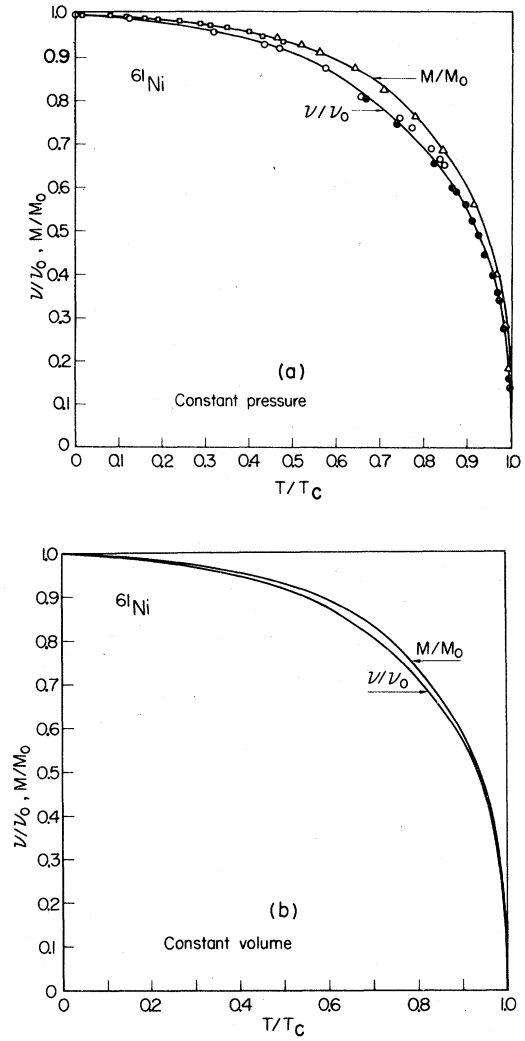

FIG. 2. Normalized NMR frequency $\nu(T)/\nu_0$ and magnetization $M(T)/M_0$ of ferromagnetic nickel vs temperature. (a) At constant pressure: ●—present data; ○—Streever and Bennett; (Ref. 8) Δ—Weiss and Forrer (Ref. 75); □—Kaul and Thompson (Ref. 76). (b) At constant volume.

tion. This has already been shown for nickel by Riedi[31] and by Streever and Bennett[8] in the temperature range 4.2 to 300 K. Thus we can make a least-squares fit of $\nu(T)$ at constant volume to the power law $\nu(T)/\nu_0 = M(T)/M_0 = B\epsilon_-^{\beta}$. This constant volume fit yielded values of the parameter B, the critical exponent β and T_c given in Table III. There is a small change from the values of B in Table I but β and T_c remain practically the same. This is not surprising because the parameters are deduced from a small range of temperature $\epsilon_- \ll 1$, where the volume changes are small.

TABLE II. Parameters used for correction of frequency and magnetization to constant volume. Logarithmic derivatives are in units of 10^{-7}/bar.

Metal	$(\partial \ln V/\partial P)_T$	$(\partial \ln \nu/\partial P)_T$	$(\partial \ln M/\partial P)_T$
Nickel	−5.32[a]	9.4[b]	−2.9[c]
Cobalt	−5.28[a]	6.13[d]	−2.18[e]

[a]P. W. Bridgman, *Physics of High Pressures* (Bell, London, 1949), p. 167.
[b]Reference 26.
[c]Reference 28.
[d]R. V. Jones and I. P. Kaminov, Bull. Am. Phys. Soc. 5, 175 (1960).
[e]Reference 27.

In the case of iron, the hyperfine-field coupling has been found to have a substantial explicit temperature dependence between 4.2 and 300 K.[26] This effect can be represented by $C = C_0(1 - 0.77 \times 10^{-7}T^2)$. Thus constant volume plots of M/M_0 and ν/ν_0 show considerable differences in the intermediate temperature range. We have not carried out a constant volume power-law fit for the critical region of iron. Our experience with cobalt and nickel suggests that the effect of volume corrections to the critical exponent is small. Likewise, the effect of the explicit temperature dependence of the hyperfine coupling is negligible compared with other sources of experimental error.

IV. KNIGHT SHIFTS IN THE PARAMAGNETIC STATE

The Knight shift (K) was measured in paramagnetic nickel from 1173 down to 723 K ($\epsilon_+ \equiv T/T_c - 1 \simeq 0.15$). Measurements in solid

TABLE III. Power-law parameters for the critical behavior of the spontaneous magnetization at constant volume.

Metal	B	β	T_c (K)
Nickel	1.3±0.05	0.355±0.014	632.7±0.4
Cobalt	1.18±0.05	0.308±0.012	1394.8±1.0

paramagnetic cobalt covered the range from the melting point (1768 K) down to 1570 K ($\epsilon_+ = 0.13$) and in the liquid extended from 1825 down to 1692 K in the supercooled range. These data are shown in Fig. 3 together with the earlier results of Segransan *et al.*[14,15] for solid and liquid nickel and the preliminary cobalt results of El-Hanany and Warren.[10] It should be noted that Segransan *et al.* obtained shifts that were in agreement with our results at their lowest temperatures near 800 K, but above 900 K their reported shifts are lower than ours by about 0.5%. We shall discuss this discrepancy in more detail shortly. In the case of cobalt, there is a small systematic difference between the data of Ref. 10 obtained with powdered samples and the present bulk sample results. We attribute this to a larger temperature error (~5 K) associated with the larger thermal gradient present in the apparatus used for the earlier measurements. For both metals the strongly divergent character of the shift is evident on approaching T_c. The negative sign of the diverging shift is, of course, a consequence of the negative core-polarization hyperfine field of the d-electron spins.

As shown by Clogston, Jaccarino, and Yafet,[32] considerable additional information can be derived from the Knight shift by correlating the shift with the magnetic susceptibility. The temperature-dependent shift for a two band (s and d) model can be written

$$K(T) = K_s + K_d(T) + K_{\text{orb}} , \tag{3}$$

where K_s is the contact contribution to the Knight shift due to the s band electrons, $K_d(T)$ is the contact contribution through the core-polarization interaction of d-band electrons, and K_{orb} is the orbital contribution to the Knight shift of the whole d band.

In a similar way the magnetic susceptibility can be written as

$$\chi(T) = \chi_{\text{dia}} + \chi_p^s + \chi_p^d(T) + \chi_{vv} , \tag{4}$$

where χ_{dia} is the core diamagnetism, χ_p^s and $\chi_p^d(T)$ are the Pauli paramagnetism of the s and d bands, respectively, and χ_{vv} is the orbital paramagnetic susceptibility which is the analog of the Van Vleck temperature-independent paramagnetism.[33] Thus Eqs. (3) and (4) can be combined to yield

$$K(T) = \alpha_s \chi_p^s + \alpha_d \chi_p^d(T) + \beta' \bar{F}_j \chi_{vv} , \tag{5}$$

where $\alpha_s = 1.79 \times 10^{-4} A\,\Omega H_{\text{hf}}(s)$, $\alpha_d = 1.79 \times 10^{-4} A\,\Omega H_{\text{hf}}(d)$, and $H_{\text{hf}}(s)$ and $H_{\text{hf}}(d)$ are the hyperfine fields per electron. In Eq. (5) all χ's are volume susceptibilities and therefore $A\,\Omega$ is the molar volume, where A is Avogadro's number and Ω is the atomic volume. Similarly $\beta' = (\Omega/\mu_B) \times H_{\text{hf}}(\text{orb})$, where $H_{\text{hf}}(\text{orb})$ is the orbital hyperfine field per one unit of angular momentum (μ_B is a Bohr magneton). $\bar{F}_j$ is a relativistic correction factor estimated as $\bar{F}_j = 1.086$.[32]

Using the procedure of Clogston *et al.*,[32] plots of K vs χ at constant pressure were constructed for nickel

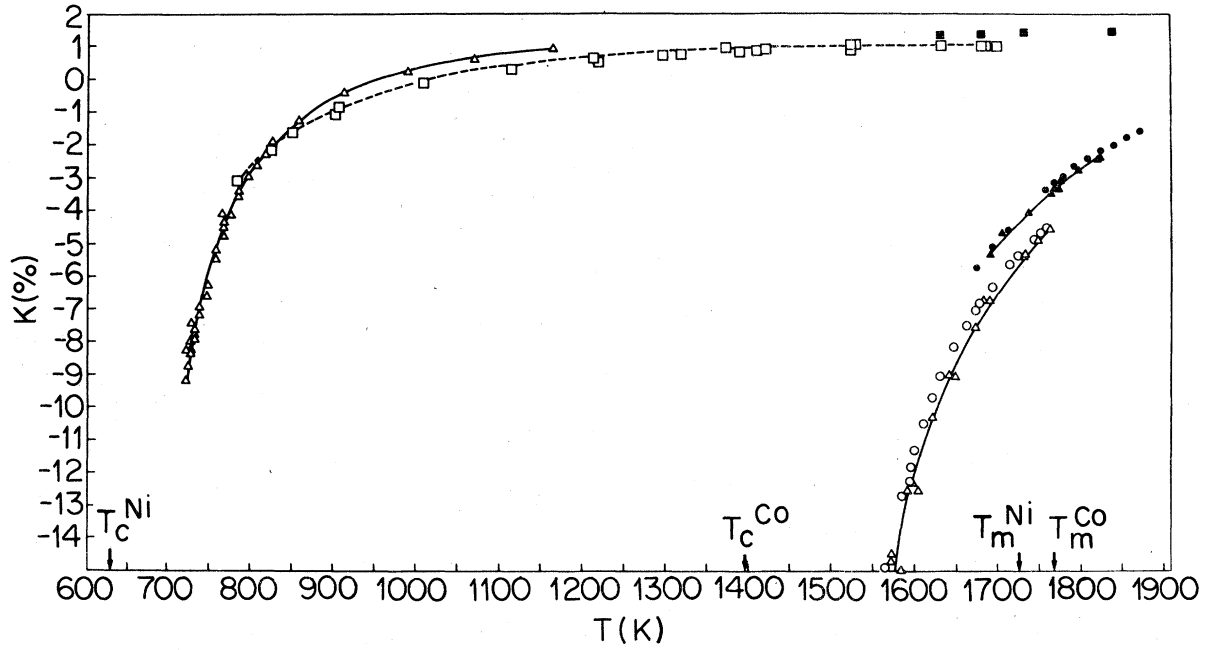

FIG. 3. Knight shift as a function of temperature in paramagnetic nickel and cobalt. Open points, solid state; closed points, liquid state. Nickel: Δ—present data; □ ■—Ref. 15. Cobalt: Δ ▲—present data; ○ ●—Ref. 10.

and cobalt. These are shown in Figs. 4 and 5, respectively. The values $K_s = 0.23\%$, $\chi_p^s \approx 10^{-5}$ emu/mole, $\chi_{dia} = -2 \times 10^{-5}$ emu/mole (Ref. 34), and $H_{hf}(orb) \approx 560$ kOe/μ_B (Ref. 35) were assumed for nickel, and χ data at constant pressure were taken from Arajs and Colvin.[36] For cobalt, the values $K_s = 0.23\%$ and $\chi_p^s + \chi_{dia} \approx 0$ (Ref. 37) were assumed. A value of $H_{hf}(orb) \approx 750$ kOe/μ_B was calculated by Freeman and Watson[35] for Co^{2+} while Dupree *et al.* give $H_{hf}(orb) \approx 440$ kOe/μ_B for cobalt impurities in a metallic host.[38] For purposes of the present analysis it is sufficient to take the average of these values, $H_{hf}(orb) \approx 600$ kOe/μ_B. The χ data for cobalt at constant pressure were taken from Urbain and Ubelacker[39] and Müller.[40] The K vs χ plots of Figs. 4 and 5 yielded the values of $H_{hf}(d)$, χ_{vv}, and K_{orb} given in Table IV. The hyperfine fields $H_{hf}(d)$ were determined from least-squares fits of the $K - \chi$ data, and the values of χ_{vv} and K_{orb} were obtained from the intercepts shown in Figs. 4 and 5.

The lower (more negative) shift values obtained by Segransan *et al.*[14,15] for nickel above 900 K are clearly evident in Fig. 4. The 20% difference in values of $H_{hf}(d)$ given in Table IV is a direct consequence of this experimental discrepancy. The data of Segransan *et al.* yield a nonlinear $K - \chi$ plot at high temperatures, a characteristic which is not evident in our data which yield a good linear fit over the entire range. However, our data do not extend to the region of the melting point and liquid where the nonlinearity of the data of Segransan *et al.* is most pronounced. Those authors argue that the nonlinearity of their $K - \chi$

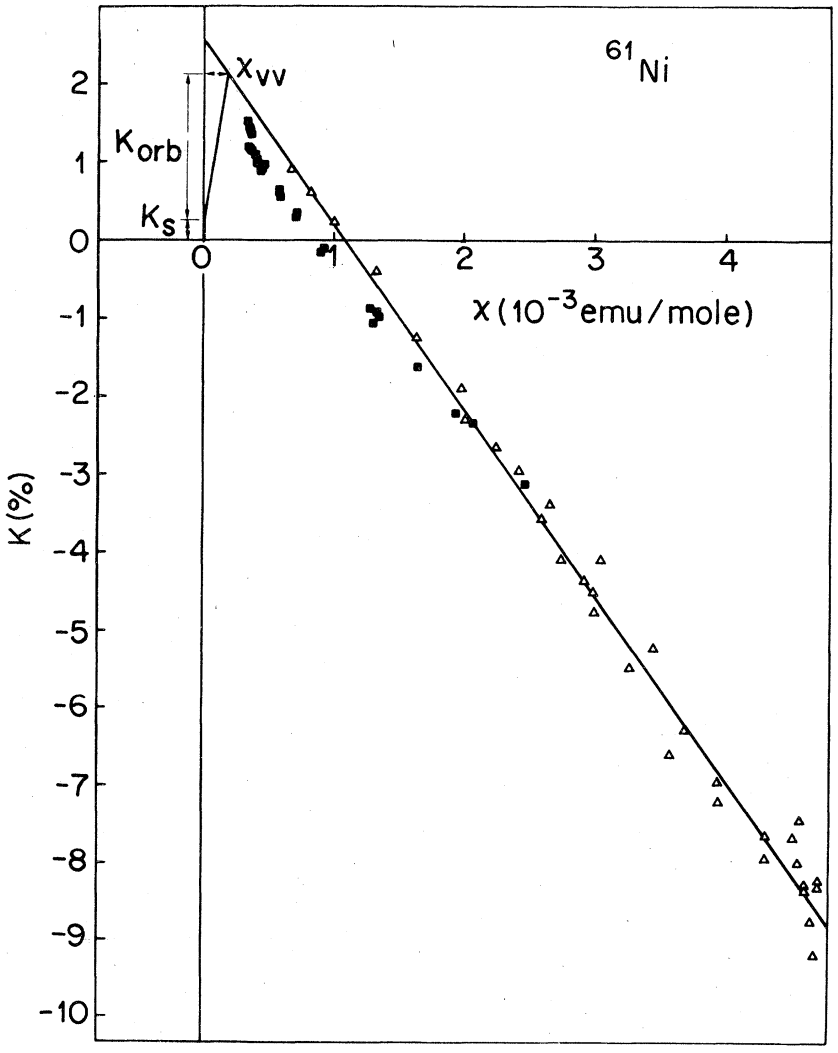

FIG. 4. Knight shift, K, vs molar susceptibility χ for paramagnetic nickel at constant pressure: Δ—present data, ■—Segransan *et al.* (Ref. 15).

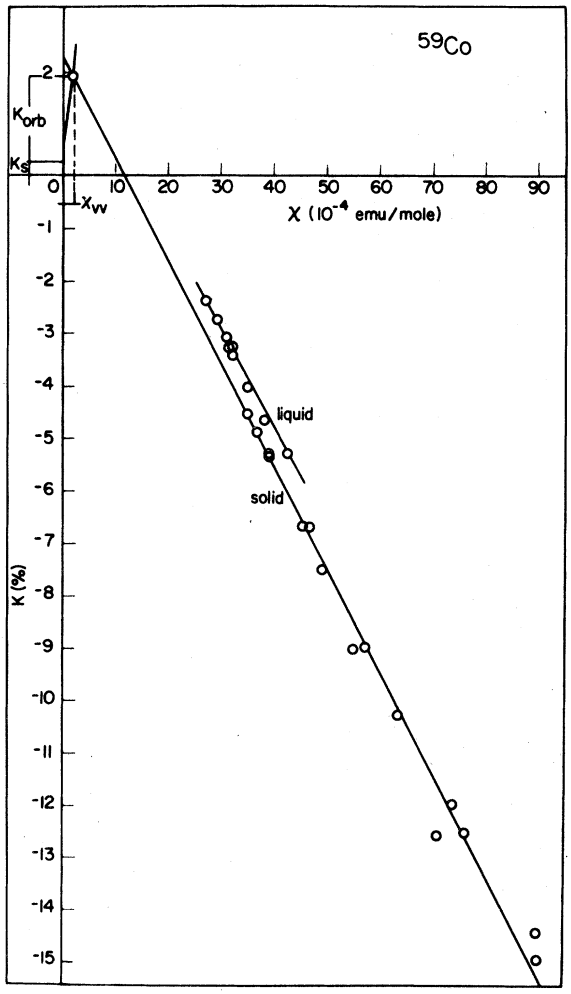

FIG. 5. Knight shift, K, vs molar susceptibility χ for paramagnetic cobalt at constant pressure.

plot is a result of a temperature-dependent orbital hyperfine field associated with thermal expansion at high temperatures.

A possible source for the discrepancy between our results and those of Segransan *et al.* was suggested by those authors to be errors in our temperature determinations, possibly due to rf heating effects.[15] We point out, however, that reconciliation of the two sets of data would require a temperature adjustment of about 250 K at the high-temperature limit of our data. Such a large temperature error cannot be present in light of the calibration and checks on rf heating effects described in Sec. II. Similarly, a large temperature error in their measurements is seemingly inconsistent with the calibration procedures described by Segransan *et al.*

Other possible sources of error do not provide a ready explanation of the discrepancy. The Knight-shift difference corresponds to a magnetic field shift of nearly 200 Oe at the fields used in our experiments. An error of this magnitude in determining the magnetic field at resonance is well outside the bonds imposed by our field calibration, including any effects due to the furnace and heater current. A similar claim was made by Segransan *et al.*

The most important difference in experimental method in the two studies was the nature of the samples themselves. In our case, the sample was a single piece of enriched ^{61}Ni metal contained in a closed quartz ampoule under an argon atmosphere. Segransan *et al.* employed powdered samples, mixed with alumina powder to provide separation, and held in an open tube exposed to the furnace atmosphere—either argon or vacuum depending on the temperature range. Estimates of the demagnetization factor correction for the two cases show that this effect is insufficient to account for the discrepancy. On the other hand, our experience with high-temperature NMR furnaces has shown that it is difficult to reduce the residual oxygen contamination at high temperatures to a level comparable with that achieved in a sealed quartz ampoule. This effect and the large surface area of the powdered sample suggest that sample oxidation should be considered as a possible problem with the experiments of Segransan *et al.* We emphasize, however, that at the present time there is no clear identification of a source of systematic error in either set of experiments.

Finally, we consider the relationship of the hyperfine fields measured in the paramagnetic and ferromagnetic states. The d hyperfine field derived

TABLE IV. Values of the d-spin hyperfine field, $H_{hf}(d)$, the orbital Knight shift, K_{orb}, and the orbital susceptibility, χ_{vv}, derived from K vs χ plots in the paramagnetic phase at constant pressure.

Metal	$H_{hf}(d)$(kOe/μ_B)	K_{orb} (%)	χ_{vv} (emu/mole)
Nickel[a]	-137 ± 7	1.9 ± 0.2	$(0.19\pm0.05)\times10^{-3}$
Nickel[b]	-113 ± 5	. . .	. . .
Cobalt[a]	-109.2 ± 6.0	1.7 ± 0.2	$(0.15\pm0.02)\times10^{-3}$

[a]Present work. [b]Reference 15.

TABLE V. Comparison of paramagnetic phase hyperfine coupling, $H_{hf}(d)$, with hyperfine field in ferromagnetic phase, $2\pi\nu_0/n_B\gamma$, and theoretical free ion value, $[H_{hf}(d)]_{fi}$. Paramagnetic state values of $H_{hf}(d)$ are corrected to 0 K volume. Right-hand columns give values of orbital Knight shift, K_{orb}, and orbital susceptibility, $\chi_{\nu\nu}$, for paramagnetic phase at constant volume.

Metal		$H_{hf}(d)$ (kOe/μ_B)	ν_0 (MHz)	$\gamma/2\pi$ (kHz/Oe)	n_B	$2\pi\nu_0/n_B\gamma$ (kOe/μ_B)	$H_{hf}(d)_{fi}$	K_{orb} (%)	$\chi_{\nu\nu}10^{-3}$ (emu/mole)
Ni		-140 ± 8	28.47	0.379	0.602	-128.3	-125	1.84 ± 0.2	0.18 ± 0.05
Co	solid	-121 ± 7	217.2	1.003	1.752	-127.1	-125	1.5 ± 0.2	0.14 ± 0.04
	liquid	-128 ± 7						2.1 ± 0.2	0.18 ± 0.05

from the $K-\chi$ plot can be compared with the ferromagnetic hyperfine field $2\pi\nu_0/\gamma n_B$ where n_B is the measured average moment per atom at 0 K in units of μ_B. However, the $K-\chi$ plots of Figs. 4 and 5 correspond to constant pressure and the effects of thermal expansion should be taken into account for a comparison with the hyperfine field at 0 K.

K and χ data at constant volume were calculated using Eq. (2) and assuming that K and χ in the paramagnetic phase are analogous to ν and M in the ferromagnetic phase, respectively. This is justified for cobalt and nickel since C in Eq. (1) was found to be almost temperature independent. Thus a $K-\chi$ diagram at constant volume could be plotted and $\chi_{\nu\nu}$ and K_{orb} were rederived. These values are given in Table V. A least-squares fit of the K vs χ data at constant volume gives the $H_{hf}(d)$ values in Table V which are compared with the ferromagnetic hyperfine field $2\pi\nu_0/\gamma n_B$ and with the theoretical calculation of Bennett *et al.*[34] for $3d^n4s^0$ configuration ions. The ferromagnetic hyperfine field was calculated taking into account the contribution from the local Lorentz field, which contributes about 3% of the measured field, in the opposite direction. It is interesting to note that our value of $K_s+K_{orb}=1.74\pm0.2\%$ is in agreement with $K_s+K_{orb}=1.94\pm0.25\%$ obtained by Fekete *et al.*[37] The latter value was measured in ferromagnetic hcp cobalt metal. The paramagnetic hyperfine field, corrected for volume expansion, is in agreement with the ν_0/γ value for cobalt and is about 9% larger for nickel. This similarity of the hyperfine fields in the two magnetic phases shows that the local electronic structure is not strongly affected by the magnetic phase transition.

V. MAGNETIC EQUATION OF STATE

In order to emphasize the similarity of the ferromagnetic and paramagnetic phases of nickel and cobalt we follow Vicentini-Missoni *et al.*[41] and write an equation of state that describes both phases using the same parameters. The magnetic equation of state relates the external magnetic field H_0, the magnetization $m\equiv M/M_0$, and the temperature T,

$$H=m|m|^{\delta-1}h(x)\ , \tag{6}$$

where H is H_0 normalized to k_BT_c/μ_0 units,

TABLE VI. Summary of parameters used for equation of state.

Metal		T_c (K)	β	B	δ	H_{int} (kOe)	$E_1(k_BT_c/\mu_0)$	E_2	$h(0)$
Nickel[a]		632.7	0.355	1.3	4.48	75	0.175	1.2	0.227
Nickel[b]		626.5	0.375		4.48		0.18	0.83	0.230
Cobalt[a]	Solid	1394.8	0.308	1.18	4.93	216.5	0.687	1.2	0.90
	Liquid						0.584		0.76

[a]Present work. [b]Reference 41.

$\mu_0 = n_B \mu_B$, δ is the exponent of the critical isotherm $T = T_c$, and $h(x)$ is an analytic function of the variable $x \equiv \epsilon_+ / m^{1/\beta}$ from 0 K to infinity, with $x_0 \equiv B^{-1/\beta}$

$$h(x) = E_1[(x + x_0)/x_0] \times \{1 + E_2[(x + x_0)/x_0]^{2\beta}\}^{[\beta(\delta-1)-1]/2\beta} . \quad (7)$$

Vicentini-Missoni *et al.*[41] demonstrated the validity of Eq. (6) for the analysis of experimental data in the critical region of a number of ferromagnets and fluids. We have used the parameters B, β, H, ν_0, and T_c derived from the experimental data in the ferromagnetic phase to fit the Knight shift calculated from Eq. (6) to the experimental values calculated at constant volume, as presented previously. The magnetization m is given by $m = KH_0 / H_{\text{int}}$ where $H_{\text{int}} = 2\pi\nu_0/\gamma$. At $T = T_c (x = 0)$

$$h(0) = E_1(1 + E_2)^{[\beta(\delta-1)-1]/2\beta} . \quad (8)$$

The values of E_1 and E_2 given in Table VI were fitted to get good agreement with the experimental Knight shift as presented in Figs. 6 and 7. The calculated Knight shift depends very weakly on the external field, hence the difference between our K data and those of Segransan *et al.*[14,15] cannot result from measurements in different external fields.

Our value of E_1 is in agreement with Vicentini-Missoni *et al.*[41]; E_2 is larger than their E_2. This may be a result of our measuring K rather far from T_c while they fitted the parameters to measurements close to T_c.

The exponent δ for cobalt was calculated from[42]

$$\delta = 1 + \gamma/\beta \quad (9)$$

using our value of β and $\gamma = 1.21$.[43] As seen from Table VI, $h(0)$ in cobalt is larger than in nickel. This is predicted by the molecular-field theory with the Brillouin function which gives for $S = \frac{1}{2}$ (Ni) a value $h(0) = \frac{1}{3}$, while for $S = 1$ (Co) a value $h(0) = \frac{9}{16}$ is obtained.

VI. NUCLEAR-SPIN RELAXATION RATES

The nuclear-spin-lattice relaxation time T_1 was measured in paramagnetic nickel over the range $738 \leq T \leq 1173$ K; both T_1 and the spin-spin relaxation time T_2 were measured in several ferromagnetic nickel samples over the range $4.2K \leq T \leq 631$ K. These results are presented in Fig. 8. For cobalt, T_1 was measured in the paramagnetic liquid from 1692 K (supercooled) up to 1825 K and in the paramag-

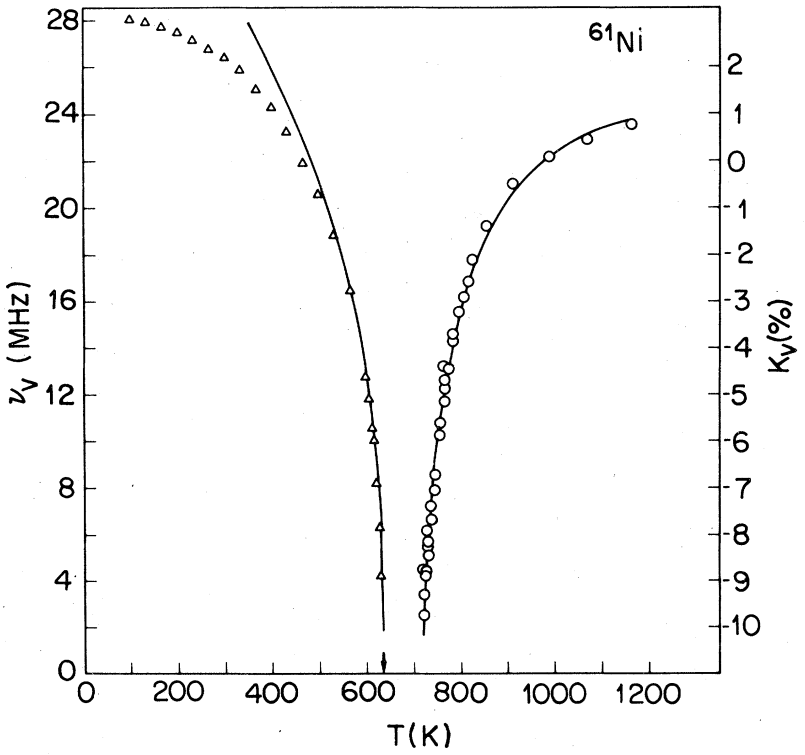

FIG. 6. Equation of state calculations (solid curves) of the Knight shift in the paramagnetic state and NMR frequencies in the ferromagnetic state of nickel at constant volume compared with the experimental results.

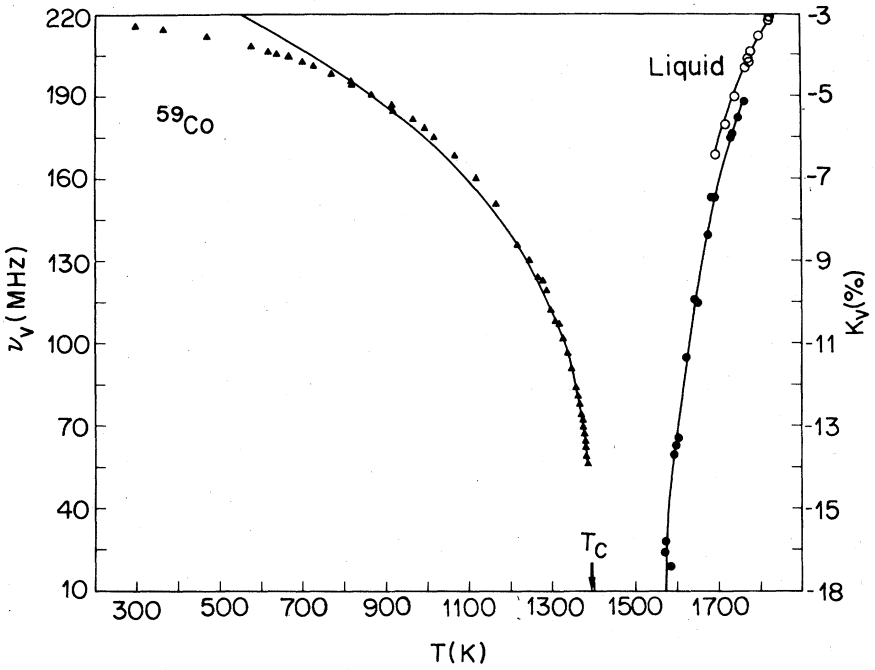

FIG. 7. Equation of state calculations (solid curves) of the Knight shift in the paramagnetic state and NMR frequencies in the ferromagnetic state of cobalt at constant volume, compared with the experimental results.

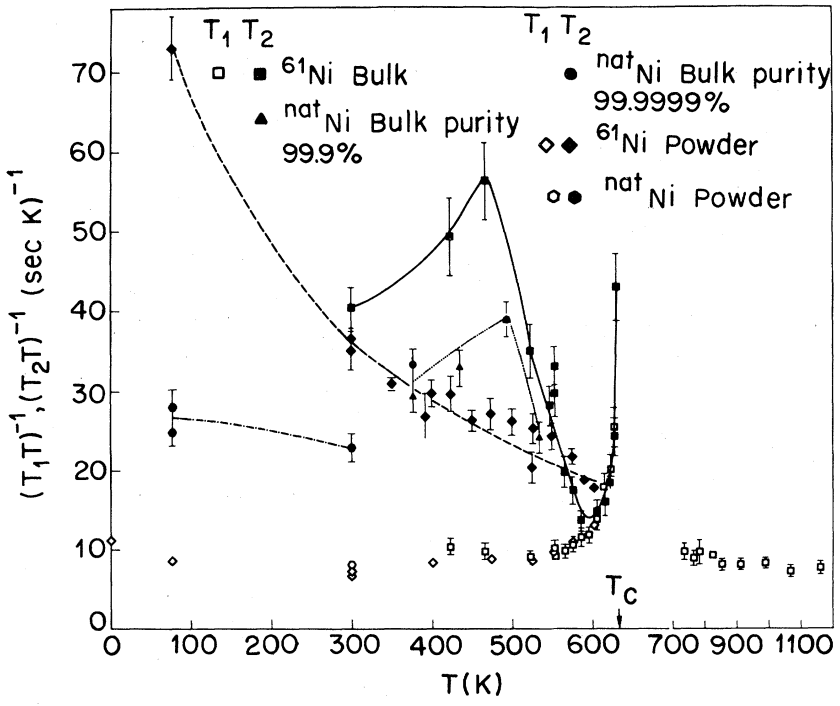

FIG. 8. $(T_1T)^{-1}$ and $(T_2T)^{-1}$ vs temperature for nickel. The curves are guides to the eye intended to indicate the difference in $(T_2T)^{-1}$ between natural and enriched samples and between bulk and powder samples.

netic solid from 1650 K to the melting point (1768 K). The data for T_1 and T_2 in ferromagnetic cobalt extend from 298 up to 1385 K. The cobalt results are presented in Fig. 9. The relaxation times for iron in the ferromagnetic state were measured from 288 up to 1027 K and are shown in Fig. 10. For each of the three metals, measurement of T_1 became progressively more difficult on approaching T_c. In the ferromagnetic phase in the temperature range closest to T_c, only T_2 could be measured.

The nuclear relaxation rates exhibit qualitatively similar behavior for all three metals. In the ferromagnetic state, the spin-lattice relaxation rates $1/T_1$ consist of a background rate for which $(T_1T)^{-1}$ is nearly constant far from T_c and a critical relaxation contribution for which $1/T_1$ diverges on approaching T_c. Well below T_c the spin-spin relaxation rates exceed $1/T_1$ but on approaching the critical region, $1/T_2 \rightarrow 1/T_1$. Within experimental error, $1/T_1 = 1/T_2$ in the critical region.

In the case of ferromagnetic nickel the data can be represented (in s^{-1}) by

$$(T_1)^{-1} = (8.0 \pm 1.0)T + (380 \pm 40)\epsilon_-^{n'} , \qquad (10)$$

where the critical exponent $n' = 0.67 \pm 0.08$. The relaxation rates in ferromagnetic cobalt are described (in s^{-1}) by

$$(T_1)^{-1} = [(0.023 \pm 0.004)T + (13 \pm 2)]T + (5400 \pm 400)\epsilon_-^{n'} \qquad (11)$$

with $n' = 0.96 \pm 0.07$. As is evident from the inset of Fig. 10, the critical relaxation rate for ferromagnetic iron cannot be described by a single power law over the full range. For $\epsilon_- \lesssim 10^{-2}$, $n' \approx 0.7$ as is the case for nickel. The background relaxation for iron is given (in s^{-1}) by

$$(T_1)^{-1} = [(1.03 \pm 0.15)(10^{-4})T + (0.061 \pm 0.005)]T \qquad (12)$$

over the range 300 to 550 K. Because the background relaxation is so low for iron, the increase in $(T_1)^{-1}$ due to spin fluctuations begins to be evident above this temperature range, even though it is still well below T_c.

In the paramagnetic state of nickel, the value of $(T_1T)^{-1}$ tends to increase on cooling toward T_c. The data can be represented [in $(sK)^{-1}$] by

$$(T_1T)^{-1} = (6.9 \pm 0.4) + (300 \pm 100)(T - T_c)^{-1} .$$

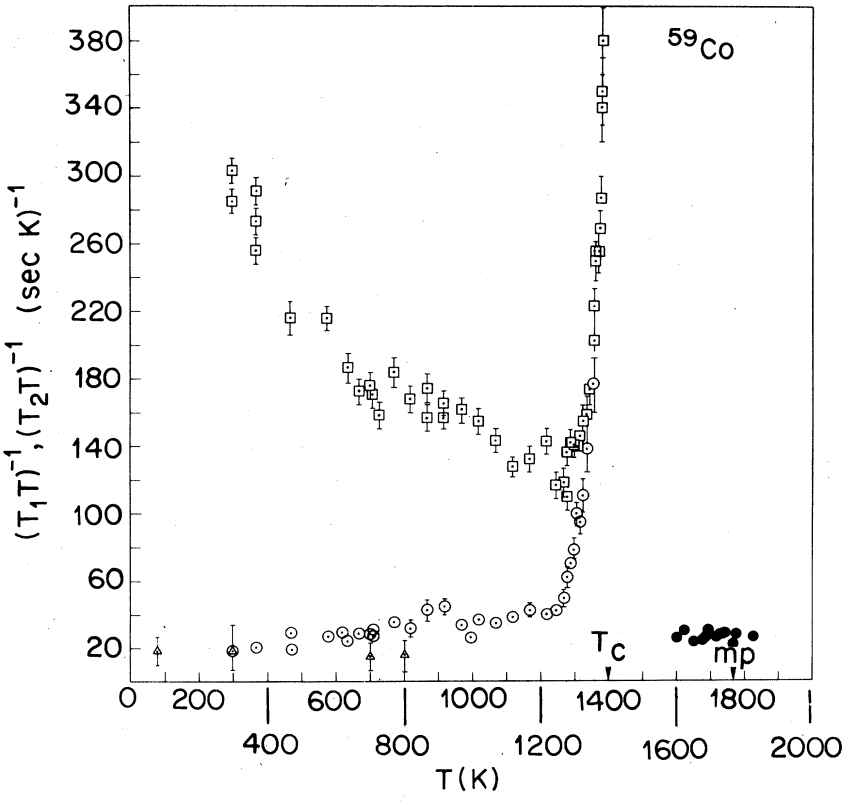

FIG. 9. $(T_1T)^{-1}$ and $(T_2T)^{-1}$ vs temperature in cobalt: circles $(T_1T)^{-1}$ in liquid (●) and solid (○) states; squares $(T_2T)^{-1}$ in solid.

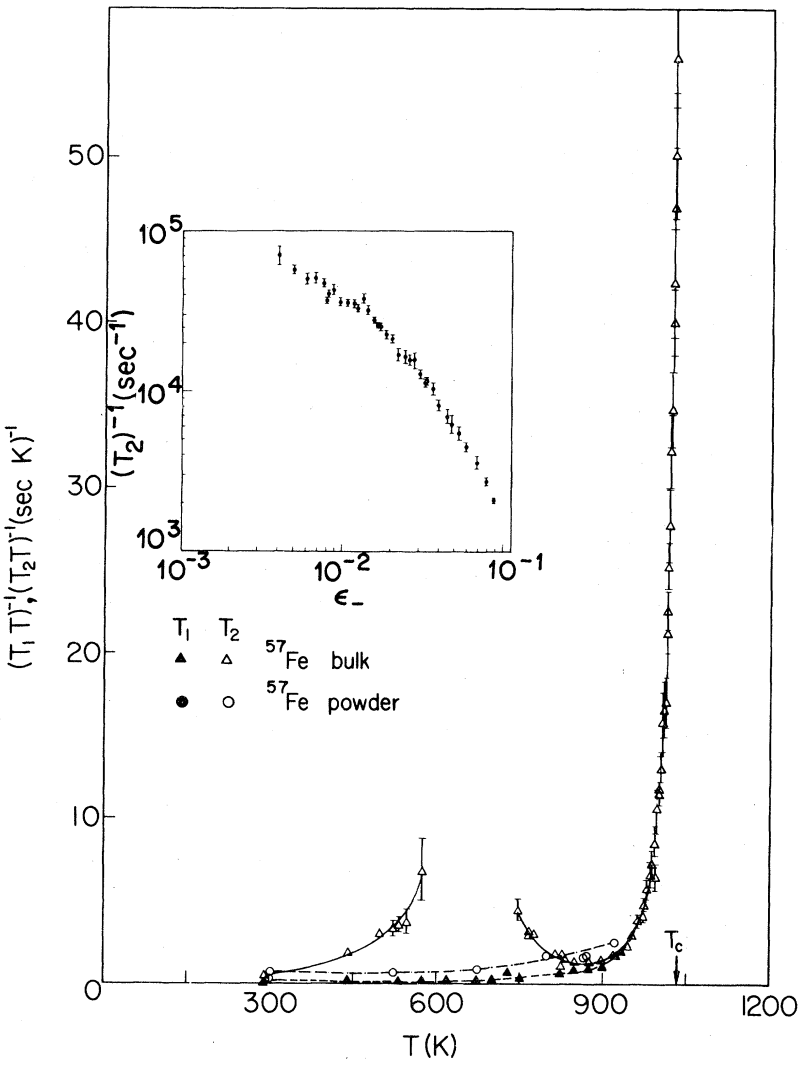

FIG. 10. $(T_1T)^{-1}$ and $(T_2T)^{-1}$ vs temperature for iron. The curves are guides to the eye intended to emphasize the difference between bulk samples and powder samples. The inset gives a plot of T_2^{-1} vs ϵ_- on a log-log scale.

For paramagnetic cobalt, $(T_1T)^{-1}$ is essentially independent of temperature over the experimental range with a value [in $(sK)^{-1}$] of

$$(T_1T)^{-1} = 27 \pm 2 \ .$$

Bulk samples of ferromagnetic nickel and iron exhibit a striking peak in $(T_2)^{-1}$ below the critical region. There is no evidence of a corresponding effect in the $(T_1)^{-1}$ data.

A. Spin-lattice relaxation (noncritical)

Outside the critical region, the main potential contributions to the relaxation rate $(T_1)^{-1}$ are the contact interaction with the s-band electrons, $(T_1)_s^{-1}$,[44] the core-polarization interaction of the d-band electrons, $(T_1)_d^{-1}$,[45] and the orbital interaction of the d electrons $(T_1)_{\rm orb}^{-1}$.[46] These are the dynamic analogs of the Knight-shift components K_s, K_d, and $K_{\rm orb}$ discussed in Sec. IV. An important difference in the case of the orbital relaxation, however, is that whereas for the shift the orbital interaction is averaged over all occupied states in the d band, the corresponding average for the relaxation is restricted to states at the Fermi level. The total relaxation rate is given by

$$(T_1)^{-1} = (T_1)_s^{-1} + (T_1)_d^{-1} + (T_1)_{\rm orb}^{-1} \ . \qquad (13)$$

Because of the linear temperature dependence associ-

ated with relaxation by electrons at the Fermi surface, we adopt the usual convention and consider the products $(T_1T)^{-1}$ in the following discussion.

Moriya[47] and Chornik[48] estimated the s contact, d-core polarization, and orbital contributions to $(T_1T)^{-1}$ in ferromagnetic iron, cobalt, and nickel, and concluded that the main contribution comes from the orbital interaction. Chornik[48] calculated $(T_1T)^{-1}=3.7$ (sK)$^{-1}$ in ferromagnetic nickel, while our results are about twice as large, $(T_1T)^{-1}=8.0\pm1.0$ (sK)$^{-1}$. Part of the difference might come from nuclei interacting with domain-wall fluctuations, since the rf fields used in our experiments mostly excite nuclei at the edge of these walls. Bancroft[49] found that $1/T_1$ is 10% lower for $H_0\approx5$ kOe, a field large enough to remove the domain walls. On the other hand Walstedt[50] measured a considerably lower value $(T_1T)^{-1}=4.8$ (sK)$^{-1}$ under similar conditions. Our value of $(T_1T)^{-1}$ agrees with Walstedt's value for $H_0=0$.[50,51]

The enhancement of $1/T_1$ by domain-wall fluctuations is more important in cobalt than in nickel. The calculated value of $(T_1T)^{-1}$ for ferromagnetic cobalt is between 3 and 5 (sK)$^{-1}$,[51] in agreement with the value measured with $H_0>4\pi M$. The rate measured previously in zero field is $(T_1T)^{-1}\approx13$ (sK)$^{-1}$,[52] in agreement with our values measured at the lowest temperatures. A change of domain-wall mobility might be the cause of the weak temperature dependence of the background relaxation described by the T^2 term in Eq. (11). Alternatively, it is possible that this effect results from interactions between the nuclei and thermal magnons through the hyperfine coupling.

The background relaxation in iron exhibits a temperature dependence similar to that of cobalt up to the point at which spin fluctuations began to become important. The magnitude of the observed rate at 400 K, $(T_1T)^{-1}=0.102\pm0.010$ (sK)$^{-1}$, exceeds the calculated values[52] [0.046–0.082 (sK)$^{-1}$] by factors similar to that observed for nickel. We are not aware of any measurements of $(T_1T)^{-1}$ in iron for $H_0>4\pi M$. However the comparison with theory suggests a modest enhancement by domain-wall effects.

The calculations of the relaxation rate discussed above did not include the effects of interactions among the electrons. This is justified for the orbital contribution for which there is no exchange enhancement. Enhancement of the s-band term can be ignored since this contribution to the total relaxation is negligible, even with considerable enhancement. The d-spin core-polarization contribution while negligible far from T_c, can be strongly enhanced in the general region of the critical point. This effect is clearly evident, for example, in the results of Kontani *et al.* for $1/T_1$ in the weak itinerant ferromagnet $ZrZn_2$.[53,54] They observed a strong peak in the relaxation rate on passing through T_c in an applied magnetic field. At higher fields, the peak was reduced. The temperature and field dependences could be satisfactorily fitted to the theoretical result of Moriya and Ueda[55] for spin fluctuation enhanced relaxation in weak itinerant ferromagnets. Unfortunately this theory is not applicable to the strong itinerant ferromagnets considered in the present work. However, the broad increases of $(T_1T)^{-1}$ on approaching T_c in both ferromagnetic and paramagnetic states are qualitatively similar to the results in $ZrZn_2$.

The effect of an applied magnetic field in suppressing the enhanced relaxation provides a possible explanation for the difference between our results in paramagnetic nickel and those of Ref. 15. The values of $(T_1T)^{-1}$ we have measured at a frequency of 17 MHz are roughly 30% higher than obtained by Segransan *et al.*[15] in higher fields at 28 MHz. If the background relaxation in paramagnetic nickel far above T_c is $(T_1T)^{-1}$ as shown by the work of Segransan *et al.* this field dependence corresponds to an increase in the enhanced spin relaxation by roughly a factor 2.5 on reducing the field from 75 to 45 kOe.

B. Spin-spin relaxation (noncritical)

The measured value of $(T_2T)^{-1}$ in the ferromagnetic phase decreases with increasing temperature approaching the critical region until it is governed by the spin-lattice relaxation. The measured T_2 can be written

$$(T_2)^{-1}=(T_2')^{-1}+(T_1)^{-1}\ , \tag{14}$$

where T_2' is the relaxation time due to spin-spin interactions. Our observed values of $(T_2')^{-1}$ are given in Figs. 11, 12, and 13 for nickel, cobalt, and iron, respectively. There it can be seen that $(T_2')^{-1}$ gradually increases with temperature well below T_c, but drops abruptly on approaching the critical temperature.

There are two potentially important spin-spin interactions that will be discussed here: the Suhl-Nakamura (SN) interaction and the dipolar interaction. One can visualize the indirect SN interaction between two nuclear spins in a magnetic medium by considering the following process: a nuclear-spin flip at site 1 creates a virtual magnon through the transverse part of the nucleus-electron hyperfine interaction. The virtual magnon is then annihilated by another nuclear-spin flip at site 2, through a similar interaction. This gives rise to an effective interaction between the nuclei at sites 1 and 2.

The contribution $M_2^{\rm SN}$ of the SN interaction to the second moment in the enriched samples can be written as[56,57]

$$M_2^{\rm SN}=\tfrac{1}{3}I(I+1)\sum_{j\neq i}B_{ij}^2\ , \tag{15}$$

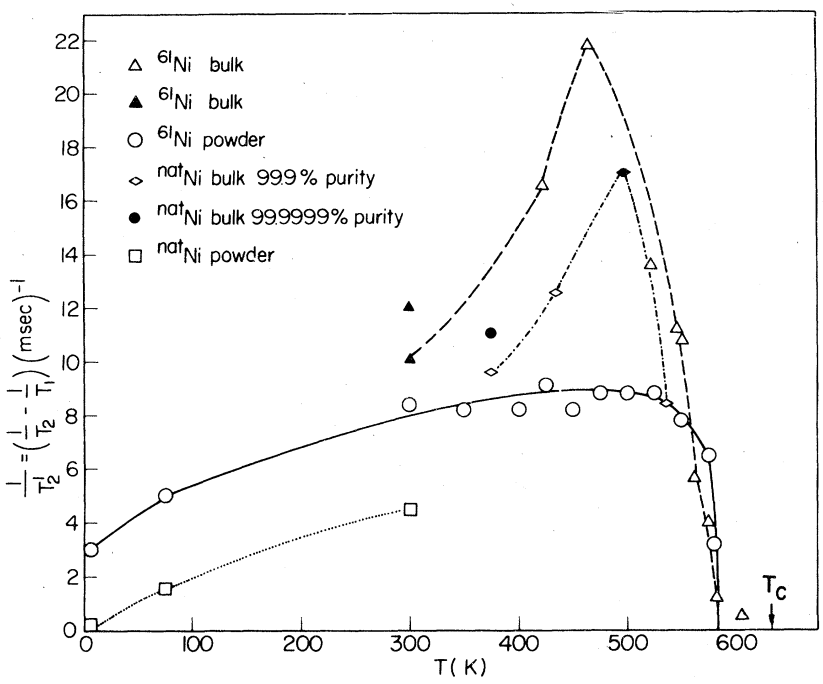

FIG. 11. Transverse relaxation rates $(T_2')^{-1}$ vs temperature in ferromagnetic nickel. The curves connect experimental results for the same samples. Note the nearly constant difference between the $(T_2')^{-1}$ for enriched and natural samples either for bulk or for a powder sample.

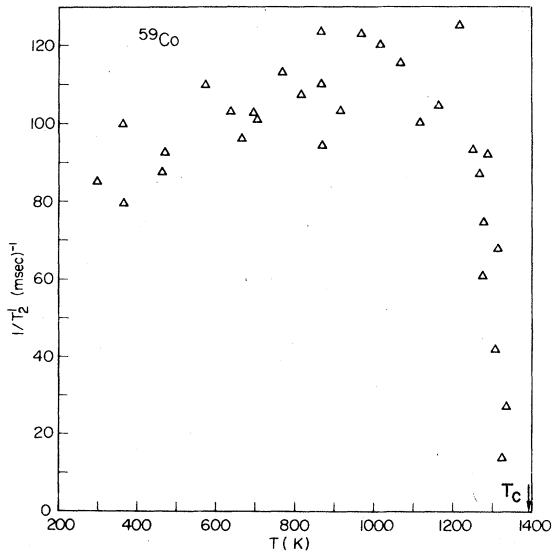

FIG. 12. Transverse relaxation rate $(T_2')^{-1}$ vs temperature for ferromagnetic cobalt.

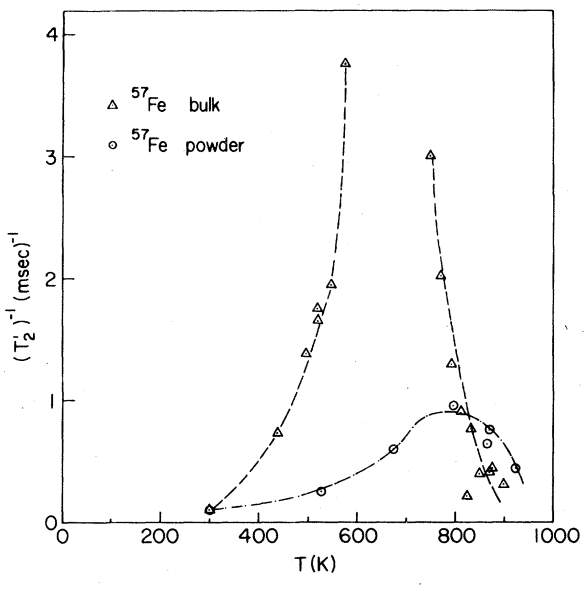

FIG. 13. Transverse relaxation rate $(T_2')^{-1}$ vs temperature for ferromagnetic iron. The curves are guides to the eye drawn through data for bulk (Δ) and powdered (○) ^{57}Fe samples.

where

$$B_{ij} = (2A^2/JZ_1n)f_{ij} \tag{16}$$

and

$$f_{ij} = (1/4\pi\alpha)e^{-\kappa r}ij/r_{ij} \ . \tag{17}$$

Here I is the nuclear spin, $A = h\nu_0/S$ is the coefficient of interaction between the nuclear and electronic spins, n is the number of sites per unit cell ($n=4$ and $n=2$ for fcc and bcc lattices, respectively), Z_1 is the number of near neighbors ($Z_1=12$ and $Z_1=8$ for fcc and bcc lattices, respectively), and

$$g\mu_B H_e = 2JSZ_1 \ , \tag{18}$$

where H_e is the exchange field. The parameter $\alpha = 2/Z_1$ is a geometric factor, and

$$\kappa = (Z_1 H_A/H_e)^{1/2} \tag{19}$$

H_A being the anisotropy field, and r_{ij} is the distance between the two nuclear spins I_i and I_j in units of lattice constant a_0. M_2^{SN} is the square of the dynamic SN linewidth. The Fourier transform of the line shape gives the decay of the echo envelope in spin-echo experiments such as ours.[58] This shape can be approximated in homogeneous samples by a Gaussian[56] with

$$T_2 \approx \hbar/(M_2^{SN})^{1/2} \ . \tag{20}$$

Substitution of Eqs. (16) and (17) in Eq. (15) gives

$$M_2^{SN} = \frac{I(I+1)A^4}{3(JZ_1n)^2 4\pi^2\alpha^2} \sum_{i\neq j} \frac{e^{-2\kappa r_{ij}}}{r_{ij}^2} = c \sum_{i\neq j} \frac{e^{-2\kappa r_{ij}}}{r_{ij}^2} \ , \tag{21}$$

where c is a constant

$$c \equiv I(I+1)A^4/48(\pi Jn)^2 \ . \tag{22}$$

The exchange field H_e can be estimated from the Rushbrook and Wood approximation.[59] For nickel with $S = \frac{1}{2}(n_B \approx gS \approx 0.6)$ and $g\mu_B H_e = 2JSZ_1 = T_c k_B/0.346$, the value is $H_e^{Ni} \approx 13.6$ MOe. For cobalt, with $S=1(n_B=1.75)$ and $g\mu_B H_e = 2JSZ_1 = T_c k_B/0.501$, we find $H_e^{Co} \approx 21$ MOe, for iron with $S=1(n_B=2.22)$ and $g\mu_B H_e = 2JSZ_1 = T_c k_B/0.479$, the result is $H_e^{Fe} \approx 16$ MOe.

The anisotropy field can be estimated by $g\mu_B S_z H_A \approx \frac{1}{2}KS_z^2$, where to a first-order approximation this equals $\frac{1}{2}KS^2\cos^2\theta \equiv \frac{1}{2}K_1\cos^2\theta$. Here K_1 is the anisotropy constant and $\cos\theta$ the cosine of the direction of the magnetization. From Birss *et al.*,[60] Sucksmith and Thompson,[61] and Kittel[62] the measured values of K_1 in nickel, cobalt, and iron, respectively, show that K_1 decreases rapidly with temperature. We estimate from their measurements that $H_A^{Ni} \approx 1$ kOe and $H_A^{Co} \approx H_A^{Fe} \approx 350$ Oe at 0 K.

Now, from Eq. (19), $\kappa \ll 1$ for these cases and the summation in Eq. (21) can be transformed to

$$M_2^{SN} = 4\pi nc \int_0^\infty e^{-2\kappa r} dr = \frac{2\pi nc}{\kappa} \ . \tag{23}$$

Substituting the above values with $I=\frac{3}{2}$ for ^{61}Ni, $I=\frac{7}{2}$ for ^{59}Co and $I=\frac{1}{2}$ for ^{57}Fe we obtain in erg^2

$$(M_2^{SN})_{Ni} \approx 1.9\times10^{-47} \ ,$$

$$(M_2^{SN})_{Co} \approx 6.1\times10^{-44} \ ,$$

$$(M_2^{SN})_{Fe} \approx 1\times10^{-47} \ .$$

We turn now to consider the effects of nuclear dipole-dipole interactions. The contribution of the dipolar interaction to the second moment for "like" spins in a powder or a polycrystalline sample is given by[63]

$$M_2^{dip} = \tfrac{3}{5}(\gamma\hbar)^4 I(I+1) \sum_{i\neq j} \frac{1}{r_{ij}^6} \ , \tag{24}$$

where the lattice sums are $\sum_{i\neq j} 1/r_{ij}^6 = w/a_0^6$ with $w = 8.4$, 29, and 116 for sc, bcc, and fcc lattices, respectively. Using $a_0 = 3.52$ Å for nickel, $a_0 = 3.537$ Å for cobalt, and $a_0 = 2.87$ Å for iron, we obtain for the enriched samples[64] in erg^2

$$(M_2^{dip})_{Ni} = 5.4\times10^{-48} \ ,$$

$$(M_2^{dip})_{Co} = 1.09\times10^{-45} \ ,$$

$$(M_2^{dip})_{Fe} = 1.6\times10^{-50} \ .$$

It is clear that the dipolar second moment is smaller than the SN contribution in all three metals and, for cobalt and iron, it is completely negligible.

In a cubic lattice[65] we can write

$$(T_2')^{-1} = (M_2^{SN} + M_2^{dip})^{1/2}/\hbar \ . \tag{25}$$

Hence the theoretical values of $(T_2')^{-1}$ are in sec^{-1}

$$(T_2')_{Ni}^{-1} \approx 4.7\times10^3 \ ,$$

$$(T_2')_{Co}^{-1} \approx 2.4\times10^5 \ ,$$

$$(T_2')_{Fe}^{-1} \approx 3\times10^3 \ .$$

The measured $(T_2')^{-1}$ values extrapolated to 0 K in Figs. 11, 12, and 13 are smaller than the calculated values, being 3×10^3 sec^{-1} and 6×10^4 sec^{-1} for nickel and cobalt, respectively, and of the order of 10^2 sec^{-1} for iron. Further the decay is exponential rather than the expected Gaussian. Hone *et al.*[56] and Barak *et al.*[57] discuss the effect of inhomogeneous broadening resulting from nonmagnetic impurities or strains in the lattice. These prevent mutual spin flips of the nuclei due to nonconservation of energy if the difference in their Zeeman energies is larger than the strength of the interaction between them. The result

is either a smaller relaxation rate with an exponential shape[56] or a sum of exponentials[57] depending on the exact form of the inhomogeneous broadening. This broadening depends on the sample preparation and thus gives different $(T_2')^{-1}$ values. Such a dependence on sample condition may be seen in the nickel data shown in Fig. 11.

When the main contribution to spin-spin relaxation is the SN interaction, as in the present case, the relaxation rate is also almost proportional to the abundance of the observed isotope. This explains why $(T_2')^{-1}$ is 10–100 times smaller in natural nickel than in enriched ^{61}Ni samples.

Normally the SN and dipolar interaction are considered to be temperature independent. However from Eqs. (19), (22), and (23) it is evident that $(T_2')^{-1}_{SN} \propto (H_e/H_A)^{1/4} \propto (JS/K_1)^{1/4}$. Far from T_c, K_1 decreases rapidly with increasing temperature[60–62] while the magnetization decreases slowly, resulting in an increasing $(T_2')^{-1}$. No measurements of K_1 have been made near T_c, to our best knowledge, but one can assume a remanent anisotropy since spin waves can still be observed near T_c. The magnetization, on the other hand, starts decreasing rapidly on approaching T_c, resulting in a sharply decreasing $(T_2')^{-1}$ as we have observed.

The observed peak in $(T_2')^{-1}$ in bulk samples which does not appear in powder samples remains a puzzle. This effect cannot arise from diffusion of impurities since it appears at rather low temperatures. Nor can it be associated with spin-spin interactions since, in this case, it should have been reduced appreciably in the bulk natural nickel samples. Thus, since there is no anomalous behavior of $1/T_1$ in this temperature range, the peak in $1/T_2$ must be related to the behavior of the longitudinal components of the electronic magnetization.

C. Critical relaxation in the ferromagnetic state

As the temperature is raised toward T_c in the ferromagnetic state, $1/T_1$ and $1/T_2$ become equal within experimental error and both diverge at the critical temperature. Power-law exponents n' for the divergent component of the relaxation are given in Table VII. For nickel and cobalt, a single exponent suffices to represent the data over the whole experimental range. Iron, on the other hand, exhibits substantial curvature on a log-log plot (inset, Fig. 10) and an exponent can only be defined over a relatively narrow range for $\epsilon \lesssim 10^{-2}$. The value of n' for iron in this region agrees with that observed for nickel. The exponent observed for cobalt is substantially larger.

Nuclear-spin relaxation in the critical region reflects the "critical slowing down" of fluctuations of the electronic magnetization as T_c is approached. These electron-spin fluctuations couple to the nuclei through the d-spin core-polarization hyperfine field $H_{hf}(d)$. The relaxation rates are determined by the correlation functions for spin fluctuations.[66]

$$G_{ij}(\vec{r};t) \equiv \langle \delta S_i(\vec{r};t)\delta S_j(0;0)\rangle \ , \tag{26}$$

where $\delta S_i(\vec{r};t)$ is the deviation from its mean value of the ith component of the spin at position $\vec{r}$ and time t. The Fourier transform of $G_{ij}(\vec{r};t)$ is the dynamic structure factor $G_{ij}(\vec{k};\omega)$. The nuclear relaxation rates are then given by

$$(T_1)^{-1} = 2[\gamma H_{hf}(d)]^2 \int d^3k G_{\pm}(\vec{k};\omega_0) \ , \tag{27}$$

$$(T_2)^{-1} = (2T_1)^{-1} + 2[\gamma H_{hf}(d)]^2 \int d^3k G_{zz}(\vec{k};0) \ . \tag{28}$$

Because the nuclear Larmor frequency ω_0 is much smaller than the characteristic fluctuation frequencies, we can take $\omega_0 = 0$ in the integrand of Eq. (27). In this limit $(T_1)^{-1}$ becomes independent of resonant frequency. Integrals identical to those of Eq. (28) govern the decay times measured by perturbed angular correlation of gamma rays (PAC) and Mössbauer linewidths.[67,68] Our observation that $T_1 = T_2$ in the critical region implies the following isotropy condition in iron, cobalt, and nickel:

$$\int d^3k G_{xx}(\vec{k};0) = \int d^3k G_{yy}(\vec{k};0) = \int d^3k G_{zz}(\vec{k};0) \ . \tag{29}$$

The critical exponent for the divergence of $1/T_1$ and $1/T_2$ is given by dynamic scaling theory in terms

TABLE VII. Dynamic critical exponents in the ferromagnetic state.

Metal	n'	z	Range
Nickel	0.67±0.08	2.01±0.12	$2\times10^{-3} \lesssim \epsilon_- \lesssim 1\times10^{-1}$
Cobalt	0.96±0.07	2.44±0.11	$7\times10^{-3} \lesssim \epsilon_- \lesssim 6\times10^{-2}$
Iron	0.63±0.12	1.95±0.18	$4\times10^{-3} \lesssim \epsilon_- \lesssim 1.5\times10^{-2}$

of a dynamic critical exponent z and the static critical exponents.[69] For the isotropic Heisenberg ferromagnet the result is

$$n' = \nu'(z - \eta - 1) \ ,$$

where $\nu' \approx \frac{2}{3}$ and $\eta \approx 0$. Thus

$$\eta' \approx \tfrac{2}{3}(z-1) \ . \tag{30}$$

The dynamic exponent can be expressed in terms of β and ν',[69]

$$z = 3 - \beta/\nu' \ . \tag{31}$$

Thus for the isotropic Heisenberg ferromagnet the prediction of dynamic scaling theory is $z \approx 2.5$ or $n' \approx 1.0$. If, in addition to the isotropic Heisenberg coupling, the effects of non-spin-conserving (e.g., dipolar) forces are included, the so-called "modified" theory predicts $z \approx 2.0$ or $n' \approx 0.7$.[69–71]

The exponent we have observed for nickel corresponds to the predictions for the case of non-spin-conserving forces. Similar values have been obtained from PAC[67] and Mössbauer measurements[68] just above T_c. However, neutron scattering measurements[72] above T_c yield $n' \sim 1$, i.e., the pure Heisenberg exponent. This discrepancy has been discussed recently by Suter and Hohenemser.[71] They argue that the origin of the discrepancy is the different range of k values spanned by hyperfine probe studies (PAC, NMR, and Mössbauer effect) on the one hand, and inelastic neutron scattering on the other. The integrals of Eqs. (27) and (28) are weighted toward values of k smaller than the minimum accessible by neutrons and it is in this low-k range that nonconservative effects are more important. It is interesting that cobalt, with the highest Curie temperature and, hence, the strongest exchange interaction exhibits the expected Heisenberg exponent while iron, the intermediate case, exhibits crossover behavior to the nonconservative exponent close to T_c. A similar crossover has recently been reported for iron above T_c by Chow, Suter, and Hohenemser.[73]

VII. SUMMARY

By combining the use of pulsed NMR of bulk metal samples with high homogeneity high-temperature techniques, we have observed NMR up to the critical region of ferromagnetic nickel, iron, and cobalt and in paramagnetic nickel and cobalt. The experiments have yielded a number of important parameters which characterize the microscopic magnetic properties in these metals both in the critical region and at temperatures well removed from T_c.

The temperature dependence of the resonant frequency in the ferromagnetic state was analyzed to obtain the static critical exponent β for the magnetization. The values for all three metals are lower than the expected value for the isotropic Heisenberg ferromagnet and lower than those obtained by impurity hyperfine studies (e.g., *Ni*:^{100}Rh PAC[74]). While this suggests a possible systematic difference between the results of pure metal and impurity hyperfine studies, there remains uncertainty due to the fact that the impurity studies extend closer to T_c than the NMR experiments.

Analysis of the Knight shifts of ^{61}Ni and ^{59}Co in the paramagnetic states of the respective metals yielded the d-spin core-polarization hyperfine field and the orbital Knight-shift and susceptibility contributions. The hyperfine field of paramagnetic cobalt agrees with the internal field in the ferromagnetic phase, once thermal volume expansion is taken into account. For nickel, the value of $H_{\rm hf}(d)$ in the paramagnet is roughly 10% larger than the ferromagnetic value. A value reported by Segransan *et al.*[15] for paramagnetic solid and liquid nickel is smaller than the low-temperature value by about the same amount. The orbital susceptibilities of paramagnetic nickel and cobalt are roughly equal. The essential unity of the paramagnetic and ferromagnetic phases was demonstrated by fitting the ferromagnetic nuclear resonance frequencies and paramagnetic Knight shifts to a common magnetic equation of state.

The spin-lattice relaxation rates are characterized by a background process, for which $(T_1T)^{-1}$ is nearly constant, and a divergent critical relaxation contribution near T_c in the ferromagnetic state. In addition a weak spin-fluctuation enhancement of the relaxation rate was observed in the paramagnetic phase of nickel. The background rate is attributed to Korringa relaxation via the orbital hyperfine field while the critical relaxation is associated with critical fluctuations of the d-electron spins. The temperature dependence of the critical relaxation yielded the dynamic critical exponents for these ferromagnetic metals. For cobalt the behavior expected of a Heisenberg ferromagnet was observed; for nickel the exponent corresponds to the ferromagnet coupled by non-spin-conserving forces; for iron a crossover was observed with the nonconservative exponent being observed closest to T_c. The trend toward Heisenberg behavior scales with the exchange energy as indicated by the increase of Curie temperatures in the sequence Ni-Fe-Co.

The observed spin-spin relaxation rates well below th critical region are attributed to the Suhl-Nakamura indirect nuclear coupling. This coupling weakens as the magnetization drops on approaching T_c until $1/T_2$ becomes dominated by the critical relaxation. Isotropy in the critical region leads to $T_2 = T_1$. A pronounced maximum in the spin-spin relaxation rate in the subcritical range was observed in bulk samples. Except to establish that it is not related to nuclear

spin-spin interactions, we have been unable to identify the source of this effect.

ACKNOWLEDGMENTS

We wish to express our appreciation to G. Ahlers, B. I. Halperin, P. C. Hohenberg, V. Jaccarino, and N. Kaplan for valuable discussions of various aspects of this work. A. Kornblit kindly assisted with the data analysis by carrying out least-squares fits to determine critical parameters in several cases. G. F. Brennert provided valuable technical assistance throughout the experimental work carried out at Bell Laboratories. N. Kaplan, O. Eidelman, and N. Sinai generously made available their high-frequency pulsed NMR apparatus and expert assistance for measurements on ferromagnetic cobalt. We also wish to thank R. E. Walstedt for his help and the use of his apparatus in an unsuccessful search for NMR in paramagnetic iron. R. Suter and C. Hohenemser kindly provided the results of their analyses of critical exponents prior to publication. The research was supported in part by a grant from the U.S.-Israel Binational Science Foundation, Jerusalem, Israel.

---

*This work forms part of a Ph.D. thesis submitted by M. Shaham to the Weizmann Institute of Science in partial fulfillment of the requirements for the Ph.D. degree.

[1]C. Herring, in *Magnetism,* edited by G. T. Rado and H. Suhl (Academic, New York, 1966), Vol. IV, Chap. VI.

[2]M. B. Stearns, Phys. Rev. B 8, 4383 (1973); Phys. Today 31, 34 (1978).

[3]See, for example, J. Hubbard, Phys. Rev. B 19, 2626 (1979), and references therein.

[4]A. C. Gossard and A. M. Portis, Phys. Rev. Lett. 3, 164 (1959).

[5]J. I. Budnick, L. J. Bruner, R. J. Blume, and E. L. Boyd, J. Appl. Phys. 32, 1205 (1961).

[6]Y. Kôi, A. Tsujimura, and Y. Yakimoto, J. Phys. Soc. Jpn. 15, 1342 (1960); Y. Kôi, A. Tsujimura, T. Hihara, and T. Kushida, *ibid.* 17, 96 (1962).

[7]R. C. LaForce, L. E. Toth, and S. F. Ravitz, J. Phys. Chem. Solids 24, 729 (1963).

[8]R. L. Streever and L. H. Bennett, Phys. Rev. 131, 2000 (1963).

[9]M. Rotter and B. Sedlak, Czech. J. Phys. B 20, 1285 (1970).

[10]U. El-Hanany and W. W. Warren, Jr., Bull. Am. Phys. Soc. 19, 202 (1974).

[11]M. Shaham, J. Barak, U. El-Hanany, and W. W. Warren, Jr., Phys. Rev. Lett. 39, 570 (1977); 39, 851 (1977); 40, 1112 (1978).

[12]W. W. Warren, Jr., Bull. Am. Phys. Soc. 23, 226 (1978).

[13]M. Shaham, J. Barak, U. El-Hanany, and W. W. Warren, Jr., Solid State Commun. 29, 835 (1979).

[14]P. J. Segransan, W. G. Clark, Y. Chabre, and G. C. Carter, J. Phys. F 6, L153 (1976).

[15]P. J. Segransan, Y. Chabre, and W. G. Clark, J. Phys. F 8, 1513 (1978).

[16]M. Shaham and U. El-Hanany, J. Phys. E 12, 359 (1979).

[17]The experiments described in this paper were carried out in two locations—the Soreq Nuclear Research Center and Bell Laboratories. The experimental methods employed in the two laboratories were the same in most respects. We do not attempt to discuss separately the methods used or the results obtained in the two locations.

[18]M. Marshall, Phys. Rev. 110, 1280 (1958).

[19]J. D. Cohen and T. R. Carver, Phys. Rev. B 15, 5350 (1977).

[20]J. Bleck, R. Butt, R. Michaelson, S. S. Rosenblum, and W. D. Zeitz, Z. Phys. B 28, 283 (1977).

[21]H. C. Benski, R. C. Reno, C. Hohenemser, R. Lyons, and C. Abeledo, Phys. Rev. B 6, 4266 (1972).

[22]C. Hohenemser, T. Kachnowski, and T. K. Bergstresser, Phys. Rev. B 13, 3154 (1976).

[23]R. M. Suter and C. Hohenemser, J. Appl. Phys. 50, 1814 (1979).

[24]M. A. Kobeissi and C. Hohenemser, in *Magnetism and Magnetic Materials—1975,* edited by J. J. Becker, G. H. Lander, and J. J. Rhyne, AIP Conf. Proc. No. 29 (AIP, New York, 1976), p. 497.

[25]W. Rocker and R. Kohlhass, Z. Naturforsch. A 22, 291 (1967).

[26]G. B. Benedek, *Magnetic Resonance at High Pressure* (Interscience, London, 1963), p. 18.

[27]J. S. Kouvel and C. C. Hartelius, J. Appl. Phys. 35, 940 (1964).

[28]E. I. Kondorskii and V. I. Sedov, Z. Eksp. Teor. Fiz. 38, 773 (1960) [Sov. Phys. JETP 11, 561 (1960)].

[29]F. C. Nix and D. MacNair, Phys. Rev. 60, 597 (1941).

[30]S. Müller and P. Scholten, Z. Angew. Phys. 20, 498 (1966).

[31]P. C. Riedi, Phys. Rev. B 15, 5197 (1977); 20, 2203 (1979).

[32]A. M. Clogston, V. Jaccarino, and Y. Yafet, Phys. Rev. 134, A650 (1964).

[33]R. Kubo and Y. Obata, J. Phys. Soc. Jpn. 11, 547 (1956).

[34]L. H. Bennett, R. E. Watson, and G. C. Carter, Natl. Bur. Stand. J. Res. 74A, 569 (1970).

[35]A. J. Freeman and R. E. Watson, in *Magnetism,* edited by G. T. Rado and H. Suhl (Academic, New York, 1965), Vol. IIA, p. 167. The calculated atomic hyperfine field was reduced by 25% to correct roughly for the effect of the metallic environment.

[36]S. Arajs and R. V. Colvin, J. Phys. Chem. Solids 24, 1233 (1963).

[37]D. Fekete, A. Grayevskey, D. Shaltiel, V. Goebel, E. Dormann, and N. Kaplan, Phys. Rev. Lett. 36, 1566 (1976).

[38]R. Dupree, R. E. Walstedt, and W. W. Warren, Jr., Phys. Rev. Lett. 38, 612 (1977).
[39]G. Urbain and E. Ubelacker, Adv. Phys. 16, 429 (1967).
[40]M. Müller, Ph.D. disseratation (Universität Basel, 1978) (unpublished).
[41]M. Vincentini-Missoni, R. I. Joseph, M. S. Green, and J. M. H. Levelt-Sengers, Phys. Rev. B 1, 2312 (1970).
[42]J. S. Kouvel and J. B. Comly, Phys. Rev. Lett. 20, 1237 (1968).
[43]R. V. Colvin and S. Arajs, J. Phys. Chem. Solids 26, 435 (1966).
[44]J. Korringa, Physica (Utrecht) 16, 601 (1950).
[45]Y. Yafet and V. Jaccarino, Phys. Rev. 133, A1630 (1964).
[46]Y. Obata, J. Phys. Soc. Jpn. 18, 1020 (1963).
[47]T. Moriya, J. Phys. Soc. Jpn. 19, 681 (1964).
[48]B. Chornik, Phys. Rev. B 4, 681 (1971).
[49]M. H. Bancroft, Phys. Rev. B 2, 182 (1970).
[50]R. E. Walstedt (private communication).
[51]R. E. Walstedt, V. Jaccarino, and N. Kaplan, J. Phys. Soc. Jpn. 21, 1843 (1966).
[52]V. Jaccarino, N. Kaplan, R. E. Walstedt, and J. H. Wernick, Phys. Lett. 23, 514 (1966).
[53]M. Kontani, T. Hioki, and Y. Masuda, Solid State Commun. 18, 1251 (1976).
[54]M. Kontani, J. Phys. Soc. Jpn. 42, 83 (1977).
[55]T. Moriya and K. Ueda, Solid State Commun. 15, 169 (1974).
[56]D. Hone, V. Jaccarino, T. Ngwe, and P. Pincus, Phys. Rev. 186, 291 (1969).
[57]J. Barak, I. Siegelstein, A. Gabai, and N. Kaplan, Phys. Rev. B 8, 5282 (1973).
[58]See, for example, A. Abragam, *The Principles of Nuclear Magnetism* (Oxford, London, 1961), Chap. III.
[59]G. S. Rushbrook and P. J. Wood, Mol. Phys. 1, 257 (1958).
[60]R. R. Birss, G. J. Keeler, and C. H. Shepherd, Physica (Utrecht) 86-88B, 257 (1977).
[61]W. Sucksmith and J. E. Thompson, Proc. R. Soc. London Ser. A 225, 362 (1954).
[62]C. Kittel, *Introduction to Solid State Physics,* 4th ed. (Wiley, New York, 1971), p. 567.
[63]Reference 58, p. 112.
[64]For iron we use $\gamma^{57}/2\pi = 0.1376$ kHz/Oe.
[65]R. E. Walstedt, Phys. Rev. B 5, 41 (1972).
[66]Reference 58, p. 310.
[67]A. M. Gottlieb and C. Hohenemser, Phys. Rev. Lett. 31, 1222 (1973).
[68]M. A. Kobeissi, R. Suter, A. M. Gottlieb, and C. Hohenemser, Phys. Rev. B 11, 2455 (1975).
[69]B. I. Halperin and P. C. Hohenberg, Phys. Rev. 177, 952 (1969).
[70]G. B. Teitelbaum, Pis'ma Zh. Eksp. Teor. Fiz. 21, 342 (1975) [JETP Lett. 21, 154 (1975)].
[71]R. M. Suter and C. Hohenemser, Phys. Rev. Lett. 41, 705 (1978).
[72]V. J. Minkiewicz, M. F. Collins, R. Nathans, and G. Shirane, Phys. Rev. 182, 624 (1969).
[73]L. Chow, R. M. Suter, and C. Hohenemser, Bull. Am. Phys. Soc. 25, 209 (1980).
[74]C. Hohenemser, T. Kachnowski, and T. K. Bergstresser, Phys. Rev. B 13, 3154 (1976).
[75]P. Weiss and R. Forrer, Ann. Phys. 5, 153 (1926).
[76]R. Kaul and E. D. Thompson, J. Appl. Phys. 40, 1383 (1969).